processes

MDPI

*Article*

# Experimental Study on Gas Seepage Characteristics of Axially Unloaded Coal under Different Confining Pressures and Gas Pressures

**Ke Ding [1], Lianguo Wang [1,*], Wenmiao Wang [2], Zhaolin Li [2], Chongyang Jiang [1], Bo Ren [1] and Shuai Wang [1]**

[1] State Key Laboratory for Geomechanics and Deep Underground Engineering, China University of Mining and Technology, Xuzhou 221116, China; dingke@cumt.edu.cn (K.D.); ts18030019a31@cumt.edu.cn (C.J.); 02140873@cumt.edu.cn (B.R.); swang@cumt.edu.cn (S.W.)
[2] School of Mines, China University of Mining and Technology, Xuzhou 221116, China; wwmdx1108@163.com (W.W.); lzhlcumt@163.com (Z.L.)
* Correspondence: cumt_lgwang@163.com; Tel.: +86-13115225568

**Abstract:** Protective coal seam mining can not only effectively prevent coal and gas outbursts in mines, but also provide stress unloading space for the protected coal seam. The coal body in the protected coal seam might undergo deformation, internal damage and structural damage, which changes its gas seepage characteristics. This study aims to explore the variations of permeability of the coal body in the protected coal seam under axial unloading. With the coal body from the outburst coal seam in the Huaibei mining area as the research object, experiments were conducted to explore the gas seepage characteristics of axially unloaded coal body under different confining pressures and gas pressures, using the TAWD-2000 coal-rock mechanics-seepage experimental system. According to the results, with respect to the gas seepage, the variations of permeabilities of axially unloaded coal samples are closely related to their deformation and damage. As the confining pressure and gas pressure rise, the difference between the permeability at the final failure point and the initial permeability rises at a decreasing rate. The experiments fully demonstrate that the protective coal seam is technically important for the unloaded gas drainage and the coal and gas outburst prevention of the protected coal seam. Under different confining pressures and gas pressures, the permeability of axially unloaded coal varies to different extents and at different rates. The mining scheme for the protective coal seam should be designed in accordance with its confining pressure and gas pressure. This study is of guiding significance for the prevention and control of coal and gas outbursts in coal seam groups.

**Keywords:** gas drainage; unloading axial pressure; coal body; permeability characteristics; permeability enhancement



**Citation:** Ding, K.; Wang, L.; Wang, W.; Li, Z.; Jiang, C.; Ren, B.; Wang, S. Experimental Study on Gas Seepage Characteristics of Axially Unloaded Coal under Different Confining Pressures and Gas Pressures. *Processes* **2022**, *10*, 1055. https://doi.org/10.3390/pr10061055

Academic Editor: Aneta Magdziarz

Received: 27 April 2022
Accepted: 24 May 2022
Published: 25 May 2022



## 1. Introduction

China is a country with a large consumption of coal. Coal plays an important role in its energy structure and can promote economic development. As coal mining in China continues, the shallow coal resources are beginning to be exhausted, so coal enterprises are resorting to deep mining. The mining depths of the coal mines in China are increasing at a rate of 8–12 m per year. Consequently, the gas content and gas adsorption in the coal seams strengthen, while the permeability of the coal seams weakens. Coal and gas outburst accidents are more likely to occur, seriously affecting safe production in coal mines [1–4].

To prevent and control gas accidents in a safe, economical and effective way, scholars have carried out extensive experimental and theoretical research, and put forward effective prevention and control measures. Among them, the technology of protective coal seam mining is an effective method that was put into practice [5–9]. The stress states of the coal seams differ. The mining activities in a specific coal seam inevitably affect the stress and

gas pressure (GP) distribution in other coal seams. Hence, a reasonable mining sequence is the key to the production safety of coal seam groups. In the laboratory, the stress state of protected coal seams can be simplified to a condition that the confining pressure (CP) is constant, while the axial pressure (AP) is unloaded [10]. At the same time, the gas permeability of coal is an important physical property of coal. This property is greatly affected by the in situ stress state of the coal body, and the degree and pressure of gas enrichment in the coal body. Therefore, the experimental study on the gas seepage characteristics of axially unloaded coal under different confining pressures and gas pressures is of theoretical and practical significance for both the determination of a reasonable mining sequence for multiple coal seams, and the effective on-site implementation of protective coal seam mining schemes [11–14].

Zhang et al. [15] found that permeability was negatively correlated with AP and CP and positively correlated with GP, and it varied exponentially with GP. Pan et al. [16] designed a stress path of reducing CP stepwise, while loading AP stepwise. The results revealed that, in the initial stage of loading and unloading, the permeability of the intact coal body weakens; when the stress difference exceeds the yield strength of the coal sample, the fracture volume increases, resulting in capacity expansion and permeability enhancement of the coal sample. Guo et al. [17] found that the cyclic loading and unloading could cause damage to the intact coal body; the permeability of the coal sample is enhanced when the stress exceeds its yield strength; as peak stress rises and damage in the coal sample accumulates, the stress sensitivity of the intact coal body gradually decreases. Cheng et al. [18] designed mining stress paths for three stages (loading, unloading and recovery), according to different stress concentration coefficients. They found that the permeability of coal remained almost unchanged and as low as the original value in the loading stage; however, it increased exponentially in the unloading stage and decreased exponentially in the recovery stage. Li et al. [19] compared the permeability variations of different coal samples, set a stress path for cyclic stepwise loading and unloading of AP, and obtained the variations in permeability values and stress sensitivity coefficients of different coal samples. Kong et al. [20] designed an experimental path for cyclic stepwise loading and unloading of AP and CP, and analyzed the seepage law of coal samples under this path. They concluded that under the same stress state, the permeability of the fractured coal sample was two orders of magnitude higher than that of the intact coal sample, and the permeability loss of the former was significantly greater than that of the latter.

Scholars have explored the gas seepage characteristics of coal samples under different conditions, yet few researched the seepage characteristics of the axially unloaded fractured coal body [21–24]. With the axially unloaded coal body as the research object, this study is aimed at exploring the influence of axial unloading on the permeability characteristics of the coal body under different GPs, and analyzing the pressure relief and permeability enhancement effect of axial unloading on the coal body. The research results can provide theoretical support for the analysis of the characteristics of fractures and permeability variations of protected coal seams, as well as the effective implementation of an on-site mining scheme in protective coal seams.

## 2. Engineering Background

Zouzhuang Coal Mine of the Huaibei Mining Co., Ltd. is located in the southeast of the Huaibei mining area. Its east is bounded by the Shuangdui fault and the F22 new stratum; the west is bounded by the Nanping fault; the south is bounded by the outcrop line of the first limestone layer at the top of the Carboniferous Taiyuan formation, and the north is bounded by No. 27 exploration line. The mine has a simple terrain (generally high in the northwest and low in the southeast) and a single landform (mainly river plain). The mine is located in the fault block sandwiched by the northeast-trend between the Shuangdui fault and the Nanping fault. The syncline axis and the east and west wings are characterized by a high gas content, a concentrated tectonic stress and a high risk of coal and gas outbursts. The gas occurrence in the mine is obviously affected by faults. The coal-bearing strata

of Zouzhuang Coal Mine belong to the Carboniferous and Permian systems. The coal seam of the Carboniferous system is too thin for mining. The lower Shihezi formation of the Permian system is the main coal-bearing stratum in the mine, followed by the Shanxi formation. It has over 30 coal seams whose total thickness is 23.39 m on average, of which the main minable coal seams are the $3_2$, $6_2$, $7_2$ and $8_2$ coal seams.

At present, the main minable coal seam in Zouzhuang Coal Mine is the $7_2$ coal seam, which is located in the lower part of the lower Shihezi formation, 7.86–13.88 m away from the $8_2$ coal seam, with an average distance of 10.22 m. The geographical location of the coal seams is shown in Figure 1. The $8_2$ coal seam has a poor permeability, and the GP and gas content there reach 1.24 MPa and 10.80 $m^3/t$, respectively, so conventional borehole gas drainage can hardly achieve a satisfactory gas disaster control effect, or effectively realize gas drainage. In the $7_2$ coal seam, the GP is 1.01 MPa and the gas content is 8.53 $m^3/t$. Hence, its GP and outburst risk are both lower than those of the $8_2$ coal seam. To improve the permeability of the $8_2$ coal seam, the $7_2$ coal seam serves as the upper protective seam for mining, to prevent coal and gas outburst accidents.

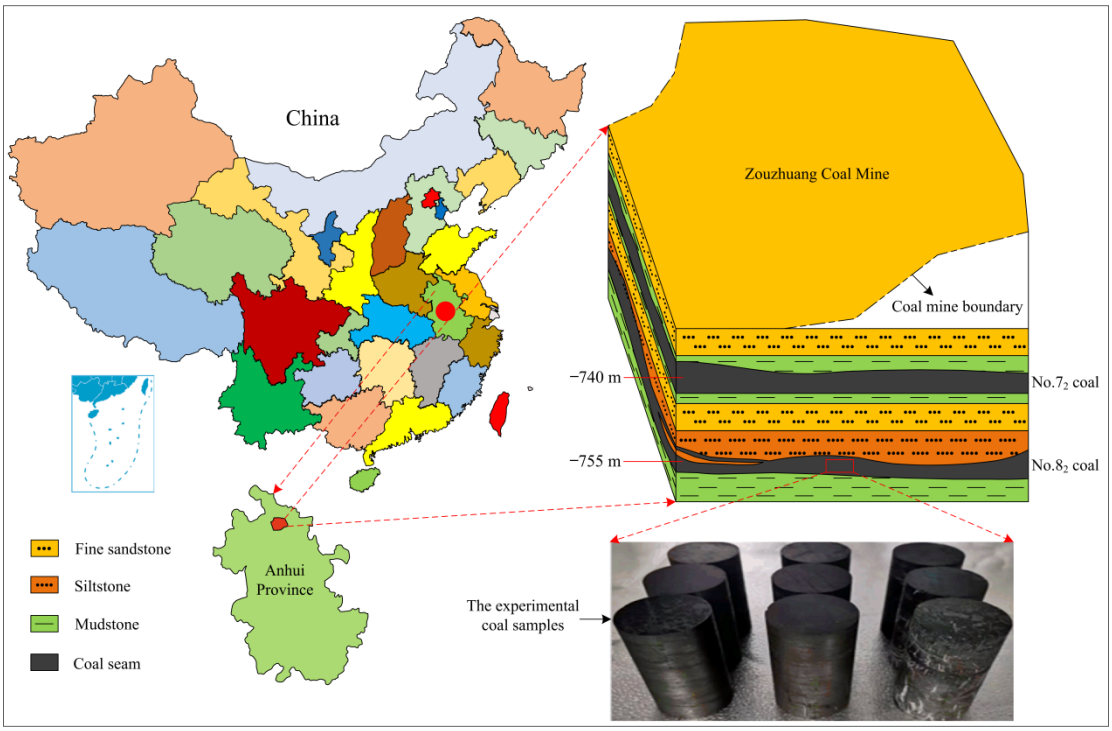


**Figure 1.** Geographical location and sampling site of the $7_2$ and $8_2$ coal seams in Zouzhuang Coal Mine.

## 3. Experimental Materials and Methods

### *3.1. Experimental Materials*

Experimental coal samples are from the $8_2$ coal seam of the Zouzhuang Coal Mine in Huaibei Mining Co., Ltd., China. The maximum original GP on the sampling site is 1.24 MPa. Coal blocks were selected from different sampling points in the same coal seam of the same mining area, sealed, saved and sent to the laboratory. According to the experimental platform and specifications, the processed coal samples were processed into cylinders with a height of 95 mm–102 mm, a diameter of about 50 mm, a parallelism of below ±0.05 mm between the upper and lower ends and a flatness of below 0.02 mm between the ends (Figure 1).

### *3.2. Experimental Equipment and Principle*

The experiments adopted the TAWD-2000 coal rock mechanics-seepage test system of the China University of Mining and Technology (Figure 2). The system consists of a pressure

host system, a pressure and temperature control system, a micro-computer operating system, etc. It can determine rock permeability under different pressures. The maximum working pressures for CP, injection pressure and AP are 70 MPa, 70 MPa and 800 MPa, respectively. The pressure fluctuation within 48 h is below 0.5%. The specifications of the TAWD-2000 device are shown in Table 1. Experiments were carried out at a constant temperature of 25 °C with $CH_4$ as the seepage medium.

**Figure 2.** Coal rock mechanics-seepage test system (TAWD-2000).

**Table 1.** The specifications of TAWD-2000 device.

| Maximum Axial Pressure/MPa | Maximum Confining Pressure/MPa | Maximum Air Pressure/MPa | Maximum Axial Displacement/mm | Force Value Test Accuracy Value/% | Displacement Test Accuracy Value/% | Overall Stiffness of the Device/(GN/m) |
|---|---|---|---|---|---|---|
| 800 | 70 | 70 | 50 | ±0.5 | ±0.5 | 10 |

The experimental principle to measure coal permeability is shown in Figure 3. According to the principle of this test system, the steady-state method was used for the permeability test. Specifically, GPs with a constant pressure difference were applied at both ends of the coal sample, so that a certain pressure gradient was maintained in the coal sample to promote gas flow through the coal fractures; meanwhile, the quantity of gas flowing through the coal sample was measured. When the flow in the coal sample stabilized to form a steady flow, the quantity of gas flowing through the coal sample in the time period was recorded, and the permeability was calculated, using the control Equation (1) [5]:

$$K = \frac{2p_0 Q L_{coal} \mu_{CH_4}}{A\left(p_1^2 - p_2^2\right)} \quad (1)$$

where $K$ is permeability, $10^{-15}$ $m^2$; $p_0$ is atmospheric pressure, 0.1 MPa; $Q$ is the quantity of gas flowing through coal briquette, $cm^3/s$; $L_{coal}$ is the length of standard briquette, mm; $\mu_{CH_4}$ is the dynamic viscosity coefficient of gas, MPa·s; $A$ is the cross-sectional area of briquette, $mm^2$; $p_1$ is the inlet pressure, MPa; $p_2$ is the outlet pressure, MPa.

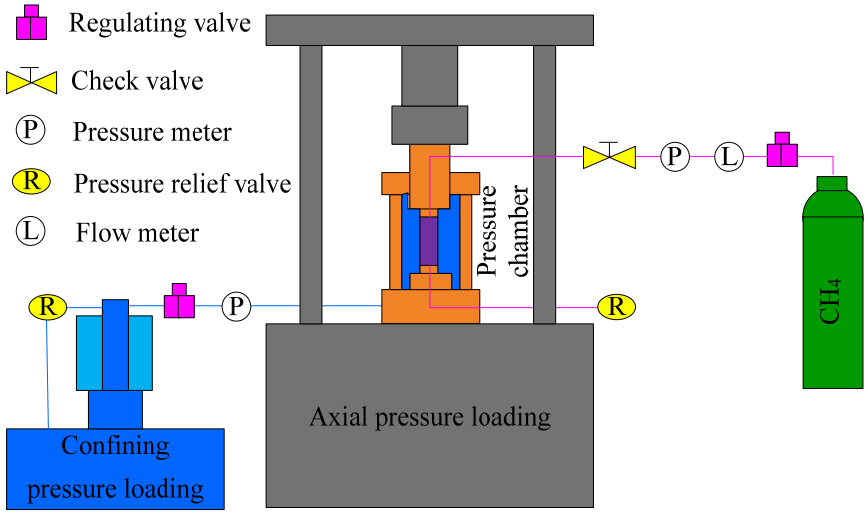


**Figure 3.** Schematic diagram of permeability measurement.

### *3.3. Stress Path and Experimental Scheme*

The coal body in the $8_2$ coal seam has experienced loading and unloading under the mining disturbance of the $7_2$ coal seam (Figure 4). That is, before its mining, the $8_2$ coal seam had experienced mining disturbance once, followed by the development of primary fractures and the emergence of new fractures. With the advancement of the $7_2$ coal seam, the upper stress decreased and the pressure on the $8_2$ coal seam was relieved. Under the influence of mining, the $8_2$ coal seam successively experienced axial compression (loading) and pressure-relief-induced dilatancy (unloading). The stress loading path is shown in Figure 5.

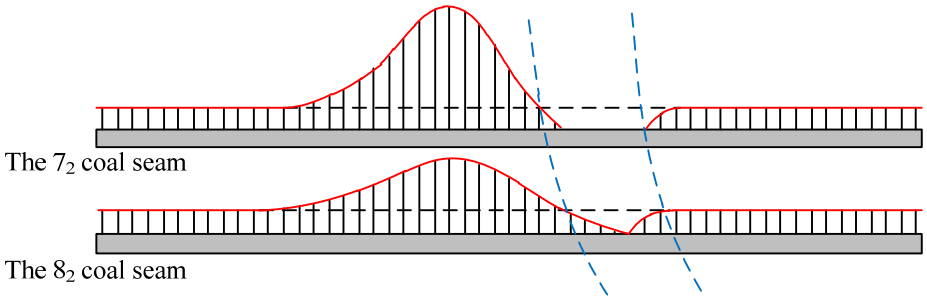


**Figure 4.** Stress distribution of the protected coal seam.

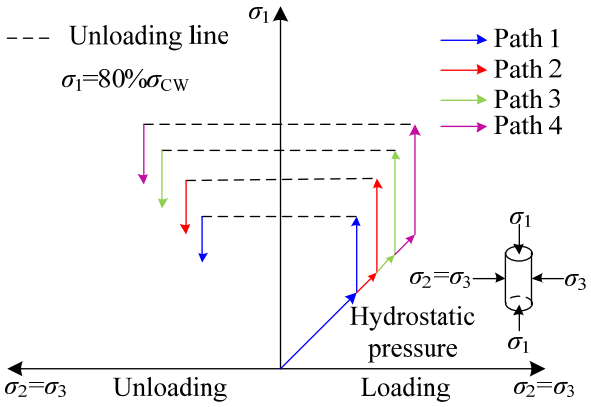


**Figure 5.** Schematic diagram of experimental stress path.

The physical and mechanical parameters of the experimental coal sample are listed in Table 2. During the experiment, first, AP ($\sigma_1$) and CP ($\sigma_2 = \sigma_3$) were loaded to 4 MPa

(hydrostatic pressure) in the control mode of 0.01 mm/s. After the pressures became stable, gas with different pressures or the same pressure was introduced. AP was continuously applied to 80% of the compressive strength of the experimental coal sample in the control mode of 0.01 N/s, in accordance with the stress path in Figure 5 and the requirements in Table 3. After the deformation and seepage of the coal sample stabilized, the GP or CP was kept unchanged. Next, AP was unloaded in the control mode of 0.01 mm/s until the coal sample finally failed, and the data collected by the data monitoring and control system were stored and analyzed.

**Table 2.** Physical and mechanical parameters of the experimental coal sample.

| Elastic Modulus/GPa | Poisson's Ratio | Tensile Strength/MPa | Cohesion/MPa | Internal Friction Angle/° | Compressive Strength/MPa |
|---|---|---|---|---|---|
| 1.60 | 0.15 | 1.09 | 1.14 | 36.61 | 14.73 |

**Table 3.** Scheme for unloading experiments.

| Scheme No. | Experimental Scheme | Experiment No. | GP/MPa | CP/MPa | Mode of Failure | |
|---|---|---|---|---|---|---|
| | | | | | Before Failure | After Failure |
| 1 | Constant GP Different CPs | XW-1 | 1.5 | 4 | 0.01 N/s | 0.01 mm/s |
| | | XW-2 | 1.5 | 5 | | |
| | | XW-3 | 1.5 | 6 | | |
| | | XW-4 | 1.5 | 7 | | |
| 2 | Constant CP Different GPs | XP-1 | 0.5 | 4 | | |
| | | XP-2 | 1.0 | 4 | | |
| | | XP-3 | 1.5 | 4 | | |
| | | XP-4 | 2.0 | 4 | | |

## 4. Experimental Results and Analysis

### 4.1. Influence of CP

According to the stress path in Figure 5 and the requirements of Scheme 1 in Table 3, the curves of stress difference and permeability variations with the axial strains of the axially unloaded coal samples under a constant GP ($p$ = 1.5 MPa) and different CPs (4 MPa, 5 MPa, 6 MPa and 7 MPa in sequence) are shown in Figure 6. In the process of axial stress unloading under different CPs, the axial strains all decline at a decelerating rate, but as CP rises, the axial strain at the final failure point displays a rising trend.

The curves of permeability and the axial strain of the axially unloaded coal samples under a constant GP ($p$ = 1.5 MPa) and different CPs (4 MPa, 5 MPa, 6 MPa and 7 MPa in sequence) are shown in Figure 7. When the CP increases from 4 MPa to 7 MPa, the permeability at the final failure point (hereafter referred to as the final permeability $K_{final}$ ) is enhanced from $1.93 \times 10^{-15}$ m$^2$ to $2.51 \times 10^{-15}$ m$^2$, by 30.05%. As the CP rises, the final permeability grows at a decelerating rate. When the CP rises from 6 MPa to 7 MPa, the final permeability is enhanced by $0.58 \times 10^{-15}$ m$^2$. Based on the data, the permeability variation of axially unloaded coal samples is shown in Figure 8a, and the final permeability $K_{final}$ is:

$$K_{final} = 0.9831\sigma_3^{0.48022}, \mathrm{R}^2 = 0.98965, (4\ \mathrm{MPa} \le \sigma_2 = \sigma_3 \le 7\ \mathrm{MPa}) \quad (2)$$

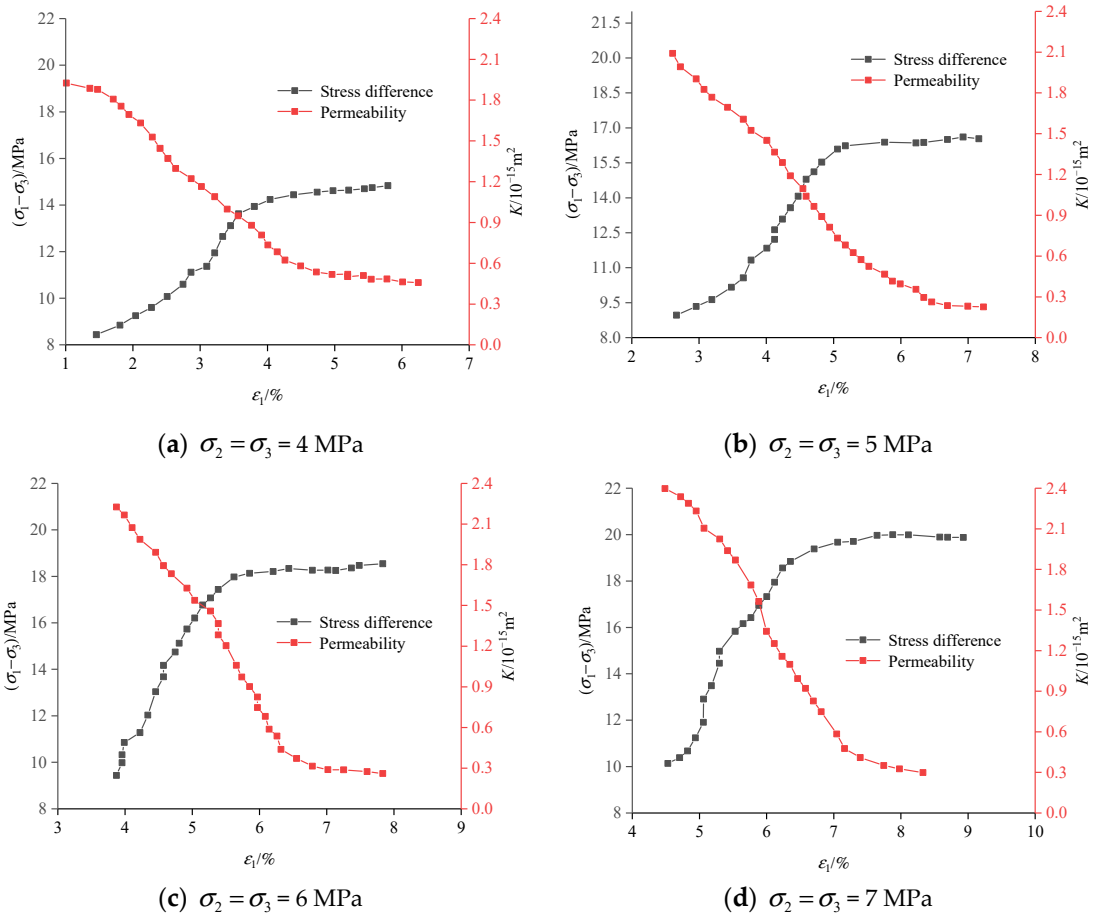


**Figure 6.** Curves of stress and permeability variations with axial strains of axially unloaded coal samples under a constant GP of 1.5 MPa and different CPs.

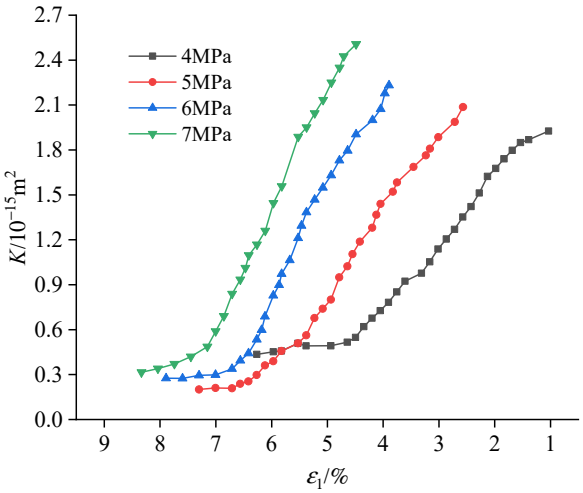


**Figure 7.** Curves of the seepage characteristics of axially unloaded coal samples under a constant GP of 1.5 MPa and different CPs.

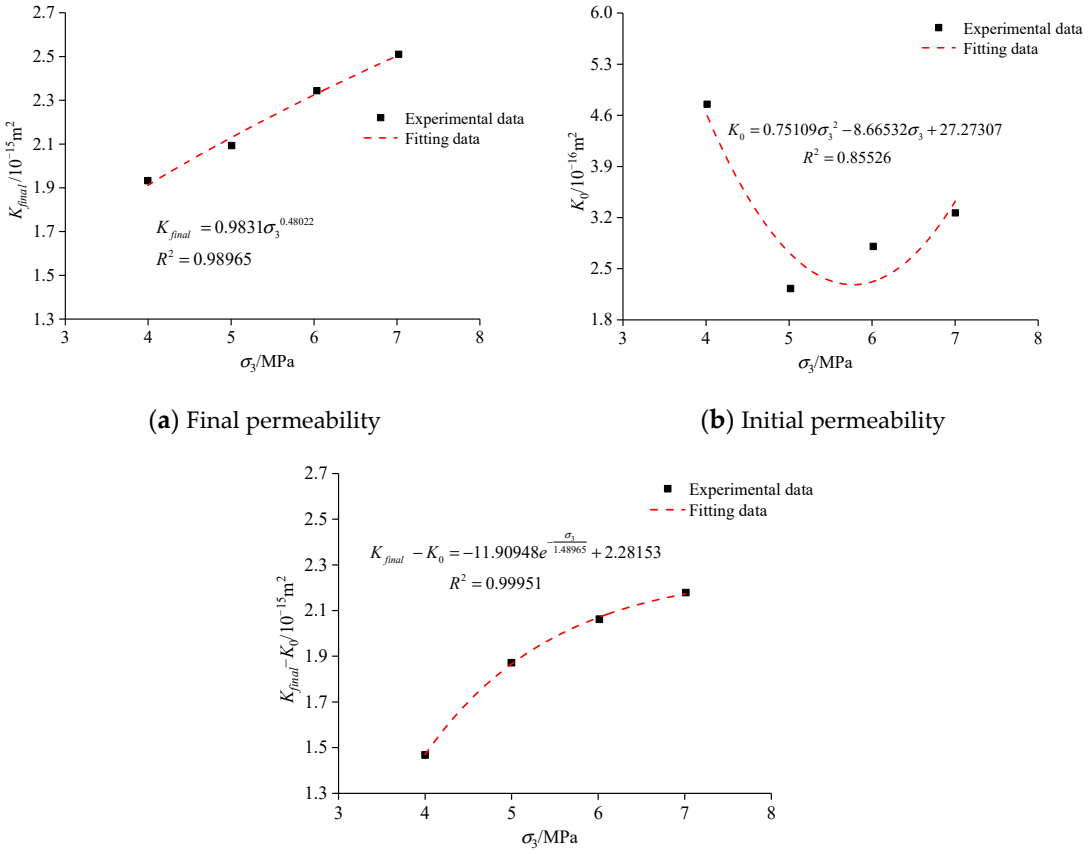


(**a**) Final permeability (**b**) Initial permeability

(**c**) Permeability difference

**Figure 8.** Permeability variations of axially unloaded coal samples under a constant GP of 1.5 MPa and different CPs.

In addition, the permeability of the coal sample before axial unloading (hereafter referred to as the initial permeability $K_0$) presents an asymmetric V-shaped variation with the increase in CP. The initial permeability reaches the lowest value ($0.22 \times 10^{-15}$ m$^2$) at 5 MPa CP. Based on the data, the initial permeability under different CPs were fitted with CP (Figure 8b), and Equation (3) was obtained:

$$K_0 = 0.75109{\sigma_3}^2 - 8.66532\sigma_3 + 27.27307, \mathrm{R}^2 = 0.85526(4\ \mathrm{MPa} \le \sigma_2 = \sigma_3 \le 7\ \mathrm{MPa}) \quad (3)$$

The difference between the final permeability $K_{final}$ and the initial permeability $K_0$ rises at a decelerating rate. Axial unloading can enhance coal permeability to a certain extent. As the CP rises, the seepage channels within the axially unloaded coal sample are gradually compacted. Therefore, the increment of permeability decreases with the increase in CP. According to the test data, the logarithmic relationship in Equation (4) was obtained by fitting the permeability difference $\Delta K$ with CP under different CPs:

$$\Delta K = -11.90948e^{-\frac{\sigma_3}{1.48965}} + 2.28153, \mathrm{R}^2 = 0.99951(4\ \mathrm{MPa} \le \sigma_2 = \sigma_3 \le 7\ \mathrm{MPa}) \quad (4)$$

The fitting coefficients $\mathrm{R}^2$ of the relationships among the final permeability, the initial permeability, the permeability difference and the CP of axially unloaded coal samples all exceed 85%, which means that the relationship between CP and the permeability of axially unloaded coal under a constant GP is well quantified.

### 4.2. Influence of GP

According to the stress path in Figure 5 and the requirements of Scheme 2 in Table 3, curves of the stress difference and permeability variations with axial strains of the axially unloaded coal samples under a constant CP ($\sigma_2 = \sigma_3$ = 4 MPa) and different GPs ($p$ = 0.5 MPa, 1.0 MPa, 1.5 MPa and 2.0 MPa in sequence) are shown in Figure 9. Under different GPs, the axial strains of the axially unloaded coal samples all decline at a decelerating rate. However, as GP rises, the axial strain at the final failure point increases.

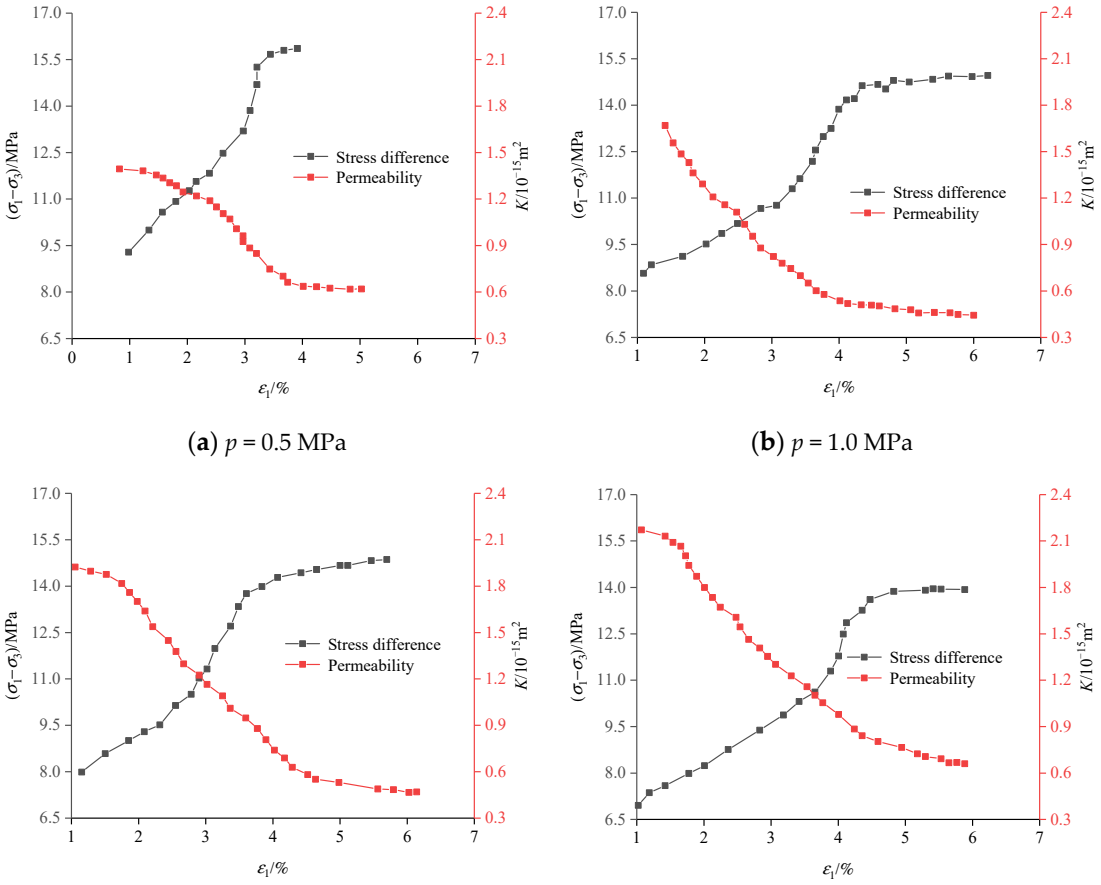


(**a**) $p$ = 0.5 MPa (**b**) $p$ = 1.0 MPa

(**c**) $p$ = 1.5 MPa (**d**) $p$ = 2.0 MPa

**Figure 9.** Curves of stress and permeability variations with axial strains of axially unloaded coal samples under a constant CP of 4 MPa and different GPs.

The curves of permeability variations with the axial strains of the axially unloaded coal samples under a constant CP ($\sigma_2 = \sigma_3$ = 4 MPa) and different GPs ($p$ = 0.5 MPa, 1.0 MPa, 1.5 MPa and 2.0 MPa, in sequence) are shown in Figure 10. When the GP goes up from 0.5 MPa to 2.0 MPa, the final permeability $K_{final}$ rises from 1.40 × $10^{-15}$ $m^2$ to 2.17 × $10^{-15}$ $m^2$; besides, the permeability difference increases from 0.78 × $10^{-15}$ $m^2$ to 1.50 × $10^{-15}$ $m^2$ by 51.21% and 92.3%, respectively, satisfying a logarithmic relationship of surging first and rising slowly later. Based on the test data, the permeability variations of axially unloaded coal samples are illustrated in Figure 11a, and the final permeability $K_{final}$ is:

$$K_{final} = 1.74635p^{-0.30173}, R^2 = 0.98889 (0.5\ \text{MPa} \leq p \leq 2.0\ \text{MPa}) \quad (5)$$

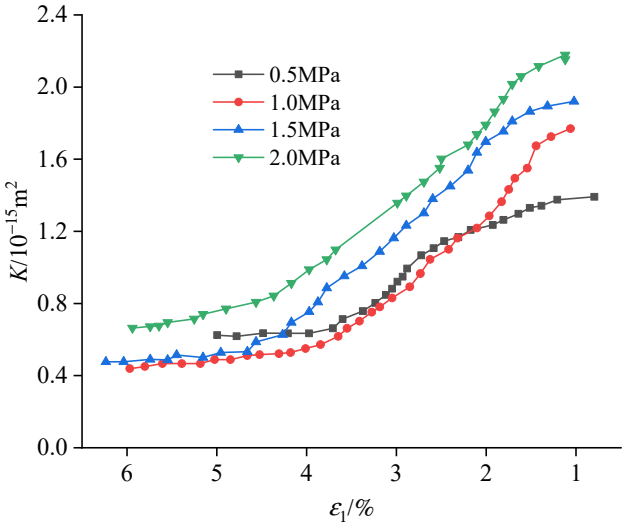


**Figure 10.** Curves of seepage characteristics of axially unloaded coal samples under a constant CP of 4 MPa and different GPs.

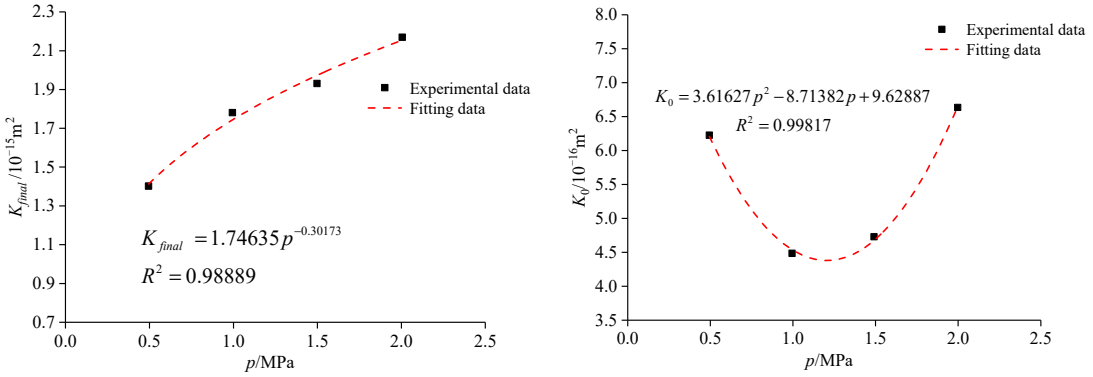


(**a**) Final permeability (**b**) Initial permeability

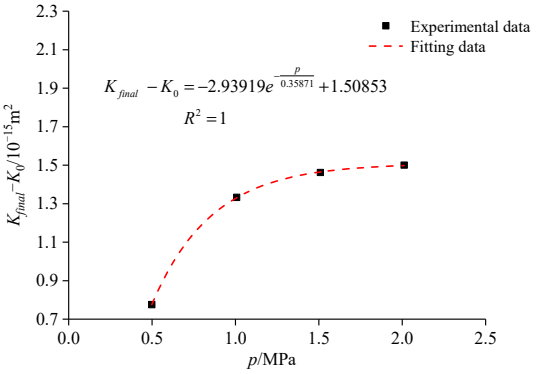


(**c**) Permeability difference

**Figure 11.** Permeability variation of axially unloaded coal samples under a constant CP of 4 MPa and different GPs.

Besides, with the rise of GP, the permeability of the coal sample before axial unloading (i.e., the initial permeability $K_0$) presents an asymmetric V-shaped variation (i.e., decreasing first and then increasing), the critical value being about 1.2 MPa. Based on the test data, the

initial permeability under different GPs was fitted with GP (Figure 11b), and Equation (6) was obtained:

$$K_0 = 3.61627p^2 - 8.71382p + 9.62887, \mathrm{R}^2 = 0.99817(0.5\ \mathrm{MPa} \leq p \leq 2.0\ \mathrm{MPa}) \quad (6)$$

The difference between the final permeability $K_{final}$ and the initial permeability $K_0$ jumps first, and then basically stabilizes. Axial unloading can enhance coal permeability to a certain extent. As GP rises, the gas adsorption and desorption of the axially unloaded coal samples gradually reach an equilibrium. Accordingly, the increment of permeability decreases gradually and stabilizes with the increase in GP. With reference to the test data, the permeability difference $\Delta K$ under different GPs were fitted with GP, and the logarithmic relationship in Equation (7) was obtained:

$$\Delta K = -2.93919e^{-\frac{p}{0.35871}} + 1.50853, \mathrm{R}^2 = 1(0.5\ \mathrm{MPa} \leq p \leq 2.0\ \mathrm{MPa}) \quad (7)$$

The fitting coefficients $\mathrm{R}^2$ of the relationships among the final permeability, initial permeability, permeability difference and GP of the axially unloaded coal all surpass 98%, suggesting that the relationship between GP and permeability values of the axially unloaded coal under a constant CP is well quantified. The fitting function can be used to predict the variation of the permeability of the axially unloaded coal under different GPs. It is expected to provide data support for the subsequent characteristic analysis on the fractures and permeability variation of the protected coal seam, and the on-site mining scheme of the protective coal seam.

## 5. Discussion

With respect to seepage, axial unloading exerts a great influence on the coal fracture structure, which determines gas seepage. Therefore, the study on gas seepage in axially unloaded coal is of significance to the prevention of coal and gas outbursts.

According to the above results, the coal body in the triaxial state mainly experiences skeleton deformation with good compactness. Its gas flow channels change slightly, leading to a low permeability. Axial unloading can cause certain damage to the coal body. As the axial load gets relieved, cracks and fractures within the coal body are gradually released, and new cracks and fractures begin to emerge in large quantities, forming a fractured coal body. As a result, gas seepage channels are released, and the slippage effect gradually emerges, which greatly enhances the permeability of the fractured coal body. Therefore, the permeabilities of the coal body under different CPs and GPs are all enhanced with the unloading of AP.

The results suggest that axial unloading exerts a considerable impact on coal permeability under different CPs and GPs, and the variations of permeability differ under different CPs and GPs. Therefore, it is crucial to establish a model that can uniformly describe the permeability of axially unloaded coal under different CPs or GPs. Moreover, axial unloading corresponding to protective coal seam mining provides a stress unloading space for the protected coal seam. Deformation, internal damage and structural damage occur within the coal body of the protected coal seam, which alters its gas seepage characteristics. Protective coal seam mining can compact and enhance the permeability of the protected coal seam. The protective coal seam, which is technically important for the unloaded gas drainage and coal and gas outburst prevention of the protected coal seam, can guide the prevention and control of coal and gas outbursts in coal seam groups. Considering that different CPs and GPs influence the axial unloading effect in varying ways, the on-site mining scheme of the protective coal seam should be adjusted, according to different CPs and GPs.

## 6. Conclusions and Suggestions

(1) When the GP is constant, the internal seepage channels of axially unloaded coal gradually get compacted with the gradual increase in CP. The difference between

the final permeability and the initial permeability rises at a decelerating rate. Under different CPs, the permeability difference follows the evolution law of $\Delta K = -11.90948e^{-\frac{\sigma_3}{1.48965}} + 2.28153$;

(2) When the CP remains unchanged, as GP gradually rises, the gas adsorption capacity of axially unloaded coal is greater than its desorption capacity, so the difference between the final permeability and the initial permeability declines first and then stabilizes. Overall, the relationship between the permeability difference and GP can be illustrated by $\Delta K = -2.93919e^{-\frac{p}{0.35871}} + 1.50853$;

(3) Axial unloading is conducive to the enhancement of coal permeability, while the permeability of axially unloaded coal varies to different extents and at different rates under different CPs and GPs. The mining scheme of protective coal seams should be designed considering the CP and GP of coal seams.

**Author Contributions:** Conceptualization, K.D. and L.W.; methodology, K.D.; software, W.W.; validation, Z.L. and C.J.; formal analysis, B.R.; investigation, S.W.; resources, L.W.; data curation, K.D.; writing—original draft preparation, K.D.; writing—review and editing, K.D.; visualization, W.W.; supervision, B.R.; project administration, C.J. All authors have read and agreed to the published version of the manuscript.

**Funding:** This research received no external funding.

**Institutional Review Board Statement:** I chose to exclude this statement.

**Informed Consent Statement:** The study did not involve humans.

**Data Availability Statement:** The data used to support the findings of this study are included within the article.

**Acknowledgments:** This study was supported by National Key Research and Development Program of China (No. 2017YFC0603004) and the support is gratefully acknowledged. This study was supported by Natural Science Foundation of Jiangsu Province, China (Grant No.BK20200628) and the support is gratefully acknowledged. This study was supported by China Postdoctoral Science Foundation funded project, (Grant No. 2020M671649) and the support is gratefully acknowledged.

**Conflicts of Interest:** The authors declare no conflict of interest.

**Notations:**

| Notation | Meaning | Company |
|---|---|---|
| $K$ | permeability | $10^{-15}$ m$^2$ |
| $p_0$ | atmospheric pressure | 0.1 MPa |
| $Q$ | the quantity of gas flowing through coal briquette | cm$^3$/s |
| $L_{coal}$ | the length of standard briquette | mm |
| $\bar{}_{CH_4}$ | the dynamic viscosity coefficient of gas | MPa·s |
| $A$ | the cross-sectional area of briquette | mm$^2$ |
| $p_1$ | the inlet pressure | MPa |
| $p_2$ | the outlet pressure | MPa |
| $\sigma_1$ | the axial pressure (AP) | MPa |
| $\sigma_2, \sigma_3$ | the confining pressure (CP) | MPa |
| $p$ | the stress gas pressure (GP) | MPa |
| $\sigma_{CW}$ | compressive strength | MPa |
| $K_{final}$ | the final permeability | $10^{-15}$ m$^2$ |
| $K_0$ | the initial permeability | $10^{-15}$ m$^2$ |
| $\Delta K$ | the permeability difference | $10^{-15}$ m$^2$ |

## References

1. Wang, F.; Li, X.; Cui, B.; Hao, J.; Chen, P. Study on the Permeability Change Characteristic of Gas-Bearing Coal under Cyclic Loading and Unloading Path. *Geofluids* **2021**, *2021*, 5562628. [CrossRef]
2. Zhang, D.; Yang, Y.; Wang, H.; Bai, X.; Ye, C.; Li, S. Experimental Study on Permeability Characteristics of Gas-containing Raw Coal Under Different Stress Conditions. *R. Soc. Open Sci.* **2018**, *5*, 180558. [CrossRef] [PubMed]

3. Li, B.; Yang, K.; Xu, P.; Xu, J.; Yuan, M.; Zhang, M. An Experimental Study on Permeability Characteristics of Coal with Slippage and Temperature Effects. *J. Pet. Sci. Eng.* **2019**, *175*, 294–302. [CrossRef]
4. Hao, D.; Zhang, L.; Ye, Z.; Tu, S.; Zhang, C. Experimental Study on the Effects of the Moisture Content of Bituminous Coal on Its Gas Seepage Characteristics. *Arab. J. Geosci.* **2018**, *11*, 436. [CrossRef]
5. Yang, Y.S.; Zhang, D.M.; Li, S.J.; Chu, Y.P.; Yang, H. Test and Analysis of Mechanics and Permeation Properties of Raw Coal. *Energy Sci. Eng.* **2019**, *7*, 868–880. [CrossRef]
6. Kai, W.; Feng, D. Experimental Investigation on Mechanical Behavior and Permeability Evolution in Coal-rock Combined Body under Unloading Conditions. *Arab. J. Geosci.* **2019**, *12*, 422.
7. Zhang, M.; Lin, M.; Zhu, H.; Zhou, D.; Wang, L. An Experimental Study of the Damage Characteristics of Gas-containing Coal under the Conditions of Different Loading and Unloading Rates. *J. Loss Prev. Process Ind.* **2018**, *55*, 338–346. [CrossRef]
8. Du, F.; Wang, K.; Wang, G.; Jiang, Y.; Xin, C.; Zhang, X. Investigation of the Acoustic Emission Characteristics during Deformation and Failure of Gas-bearing Coal-rock Combined Bodies. *J. Loss Prev. Process Ind.* **2018**, *55*, 253–266. [CrossRef]
9. Duan, M.; Jiang, C.; Gan, Q.; Li, M.; Peng, K.; Zhang, W. Experimental Investigation on the Permeability, Acoustic Emission and Energy Dissipation of Coal Under Tiered Cyclic Unloading. *J. Nat. Gas Sci. Eng.* **2020**, *73*, 103054. [CrossRef]
10. Guo, J.; Liu, J.; Li, Q.; Xu, C.; Chen, Z.; Huang, B.; Chen, S. Variation Law of Coal Permeability under Cyclic Loading and Unloading. *Therm. Sci.* **2019**, *23*, 1487–1494. [CrossRef]
11. Zhang, L.; Hao, D.; Ye, Z.; Zhang, C.; Chen, S. Experimental Study of Gas Pressure and Effective Stress Influencing on Gas Seepage Characteristics of Bituminous Coal in Both Axial and Radial Directions. *Int. J. Oil Gas Coal Technol.* **2019**, *22*, 527–553. [CrossRef]
12. Wang, K.; Guo, Y.; Xu, H.; Dong, H.; Du, F.; Huang, Q. Deformation and Permeability Evolution of Coal during Axial Stress Cyclic Loading and Unloading: An Experimental Study. *Geomech. Eng.* **2021**, *24*, 519–529.
13. Zhang, Z.; Wang, H.; Wang, L.; Zhang, D. Experimental Study on Mechanics and Permeability Properties of Water-Bearing Raw Coal Samples under In-Situ Stress. *Appl. Sci.* **2019**, *9*, 2549. [CrossRef]
14. Fan, J.; Wang, G.; Li, H.; Li, X. Studies on Gas Seepage Characteristics in Different Stress Zones of Bottom Coal in Steeply Inclined and Extra-Thick Coal Seams under Mining Action. *ACS Omega* **2021**, *6*, 34250–34262. [CrossRef]
15. Zhang, L.; Huang, M.; Xue, J.; Li, M.; Li, J. Repetitive Mining Stress and Pore Pressure Effects on Permeability and Pore Pressure Sensitivity of Bituminous Coal. *Nat. Resour. Res.* **2021**, *30*, 4457–4476. [CrossRef]
16. Pan, R.; Li, C.; Fu, D.; Xiao, Z.; Jia, H. The Study on Oxidation Characteristics and Spontaneous Combustion Micro-Structure Change of Unloading Coal under Different Initial Stress. *Combust. Sci. Technol.* **2019**, *192*, 1053–1065. [CrossRef]
17. Zhang, B.A.; Zhang, D.M.; Yang, Y.S.; Wen, D.C. Test and Study on Transfusion Law of Gas in Mining Coal. *Energy Sci. Eng.* **2019**, *7*, 179–193. [CrossRef]
18. Cheng, X.; Zhao, G.; Li, Y.; Meng, X.; Tu, Q.; Huang, S.; Qin, Z. Mining-Induced Pressure-Relief Mechanism of Coal-Rock Mass for Different Protective Layer Mining Modes. *Adv. Mater. Sci. Eng.* **2021**, *2021*, 3598541. [CrossRef]
19. Li, Q.; Liang, Y.; Zou, Q.; Li, Q. Acoustic Emission and Energy Dissipation Characteristics of Gas-Bearing Coal Samples under Different Cyclic Loading Paths. *Nat. Resour. Res.* **2020**, *29*, 1397–1412. [CrossRef]
20. Zhang, L.; Huang, M.; Li, M.; Lu, S.; Yuan, X.; Li, J. Experimental Study on Evolution of Fracture Network and Permeability Characteristics of Bituminous Coal under Repeated Mining Effect. *Nat. Resour. Res.* **2021**, *31*, 463–486. [CrossRef]
21. Kong, X.; Wang, E.; Li, S.; Lin, H.; Zhang, Z.; Ju, Y. Dynamic Mechanical Characteristics and Fracture Mechanism of Gas-bearing Coal Based on SHPB Experiments. *Theor. Appl. Fract. Mech.* **2020**, *105*, 102395. [CrossRef]
22. Yintong, G.; Lei, W.; Xin, C. Study on the Damage Characteristics of Gas-bearing Shale under Different Unloading Stress Paths. *PLoS ONE* **2020**, *14*, e0224654.
23. Zhang, D.M.; Yang, Y.S.; Chu, Y.P.; Zhang, X.; Xue, Y.G. Influence of Loading and Unloading Velocity of Confining Pressure on Strength and Permeability Characteristics of Crystalline Sandstone. *Results Phys.* **2018**, *9*, 1363–1370. [CrossRef]
24. Huang, M.; Zhang, L.; Zhang, C.; Chen, S. Characteristics of Permeability Changes in Bituminous Coal under Conditions of Stress Variation Due to Repeated Mining Activities. *Nat. Resour. Res.* **2020**, *29*, 1687–1704. [CrossRef]